SUPPLEMENTARY MATERIALS

S1. Biostratigraphic framework

Lithostratigraphic unit	Samples	Micropaleontology	Palynology	Malacology	Total
Azoic Sands Fm	-	-	-	-	**-**
Faluns and Lithothamniids Fm	5	5	-	-	**5**
Upper Sapropels Fm	3	3	3	-	**6**
Archiacina Limestones Fm	5	5	1	-	**6**
Natica Marls Fm	6	4	3	1	**8**
Lower Sapropels Fm	52	6	49	-	**55**
Chartres-de-Bretagne Fm	24	6	22	-	**28**
TOTAL	**95**	**29**	**78**	**1**	**108**

Table S1. Sample distribution and biostratigraphical analyses with regard to lithostratigraphic units. Palynology is the main analysis conducted, for the numerous organic-rich clay deposits occurrences.

Depth (m)		Index fossils (foraminifers, pollen grains, dinocysts)		Biozone or stratigraphic horizon	Age / Stage *Informal age / stage*	Num. age (Ma)	References
Min.	Max.						
0.00	4.00	-		-	Plio-Pleistocene		Van Vliet-Lanoë et al 1998
4.00	25.50	*Elphidium spp. & P. serrata* assemblage		-	Langhian to Serravallian		Margerel & Bréhéret, 1984 ; Margerel, 2009
30.00	33.00	LO of *P. armorica, N. viennoti, V. kasselensis, B. beyrichi*		Top of SBZ21 = top of P19 biozone	Rupelian	*30.3*	Cahuzac and Poignant (1997); Vandenberghe et al. (2012)
33.00	66.65	LO	*C. giuseppei, I. multispinosum, V. ceraichia*	Top of D14na		*30.6*	Köthe (2003, 2012); Köthe and Piesker, 2007.
83.20	133.66	FO		Base of D14na		*32.3*	
133.66	195.12	LO of *A. cyclops* FO of *Sl. hippophaeoides & C. simplex*		'La Rivardière / Matival' pollen assemblage	*Early Rupelian* (*Sannoisian* of the Paris Basin)	*32.3 to ca 33*	Châteauneuf (1980) Ollivier-Pierre (1980)
195.12	196.29	FO of *B. hohli, M. vanwijkei, Chloranthaceae: Chloranthus & Sarcandia sp.*		Western European biomarkers	*Earliest Rupelian*	*ca 33 to* **33.9**	Sittler et al. (1975); Châteauneuf (1980)
205.97	265.87	LO of *T. cognitus & P. crassus* FO of *T. raguhnensis, T. densus & T. rhombus*		Classic assemblage from the Paris Basin	*Late Priabonian*	**33.9** *to ca 35*	Châteauneuf (1980)
277,99	374.97	Bloom of *Hamamelidaceae and A. cyclops* FO of *P. calauensis* LO of *Diporites, R. loburgensis*		Regional markers	*Lower Priabonian*	*ca 35 to* **37.8 ± 0.5**	Châteauneuf (1980) Ollivier-Pierre (1980)
379.10	391.53	LO of *P. subhercynicus,* FO of *T. clavatus & T. sauerae*		Regional markers	*Late Bartonian*	**37.8 ± 0.5** to 38.33	Châteauneuf (1980) Ollivier-Pierre (1980) Schuler (1988)
392.32	399.88	LO of *C. parisiensis, C. columnatortilis, A. kerfornei, V. globularis, Normapolles group, Bombacacidites Spp., Nypa* FO of *R. loburgensis*		Top of SBZ17 = base of C17n3n	Top of *Biarritzian* (*middle / late Bartonian* boundary)	38.33	Châteauneuf (1980) Ollivier-Pierre (1980) Serra-Kiel et al. (1998); Vandenberghe et al. (2012)
399.88	401.70	FO of *C. parisiensis, C. columnatortilis, A. kerfornei, V. globularis*		SBZ17	*Biarritzian* (*early - middle Bartonian*)	38.33 to **41.2 ± 0.5**	Serra-Kiel et al. (1998); Vandenberghe et al. (2012)
Below 404.92 m depth is found the Brioverian Group, a folded shale series of late Neoproterozoic to early Cambrian age.							

Table S2. Depth intervals of relevant biostratigraphic limits, and corresponding numerical ages according to the GTS2012 (Vandenberghe et al., 2012). SBZ refer to Shallow Benthic Zone; D14na refer to Dinocysts biozonation from Köthe (2003); FO for First Occurrence, LO for Last Occurrence. See Bauer et al. (2016) for reference taxa. Numerical ages are either calibrated (bold) or estimated (italic). The "Biarritzian" regional stage was defined by Hottinger and Schaub (1960), the equivalence with benthic foraminifera was given by Cavelier et Le Calvez (1965). Subsequently Serra-Kiel et al. (1998) gave precisions on its stratigraphic position according to international standard (equivalent to SBZ17). In the GTS2012 (Vandenberghe et al., 2012), the top SBZ17 is coeval with the base of C17n3n. The Bartonian/Priabonian boundary is better constrained in the Borehole CDB1 than it is in the Paris Basin to which it is compared.. The Eocene-Oligocene boundary is well constrained in the Borehole CDB1, in between the LO of exclusively Priabonian assemblages and the FO of *Boehlensipollis hohli* (Sittler et al., 1975; Sittler and Schuler, 1976; Schuler and Sittler, 1976; Châteauneuf, 1980; Ionescu and Alexandrescu, 1995; King, 2016), covering a <10 m-thick interval. The D14na dinocysts subzone was defined by Köthe (2003; Köthe and Piesker, 2007), then correlated with nannofossil biozones (Köthe, 2012). The choice of this dinocyst biozonation is motivated because it is built upon recent (2000's) German data, and from a closer location to our place, together with a very good correlation between dinocysts and nannofossils. However, to ensure a consistent dataset, ages from Köthe (2012) were updated according to ages from the GTS2012. The SBZ21 was defined by Cahuzac and Poignant (1997); its top limit was correlated with top of P19 biozone from Berggren et al. (1995).

S2. Rock magnetism analyses and magnetostratigraphy

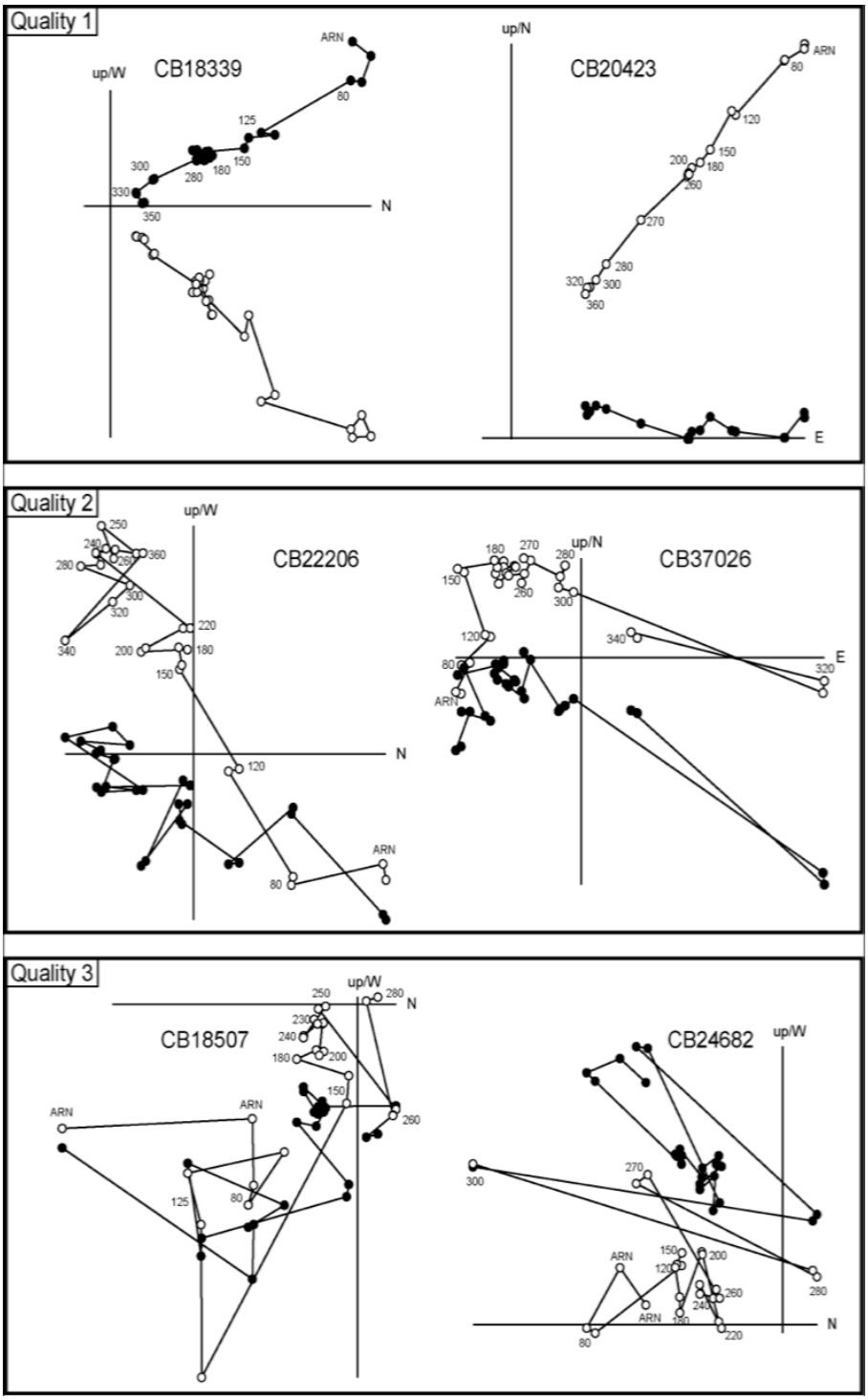

Figure S1. Charateristic thermal demagnetization diagrams. Open (full) symbols are projections in the vertical (horizontal) plane. Quality 1 (Q1) are ChRM directions of normal or reversed polarity from which a well-defined direction was determined from stable and linear demagnetization paths, yielding MAD typically below 15°. Quality 2 (Q2) directions have clearly defined normal or reversed polarities but the directions are less reliable because of paths not-fully demagnetized to the origin, directional scatter and/or overlapping secondary overprint. Quality 3 (Q3) yielded demagnetizations from which neither directions nor polarity could be interpreted and were rejected from further analyses.

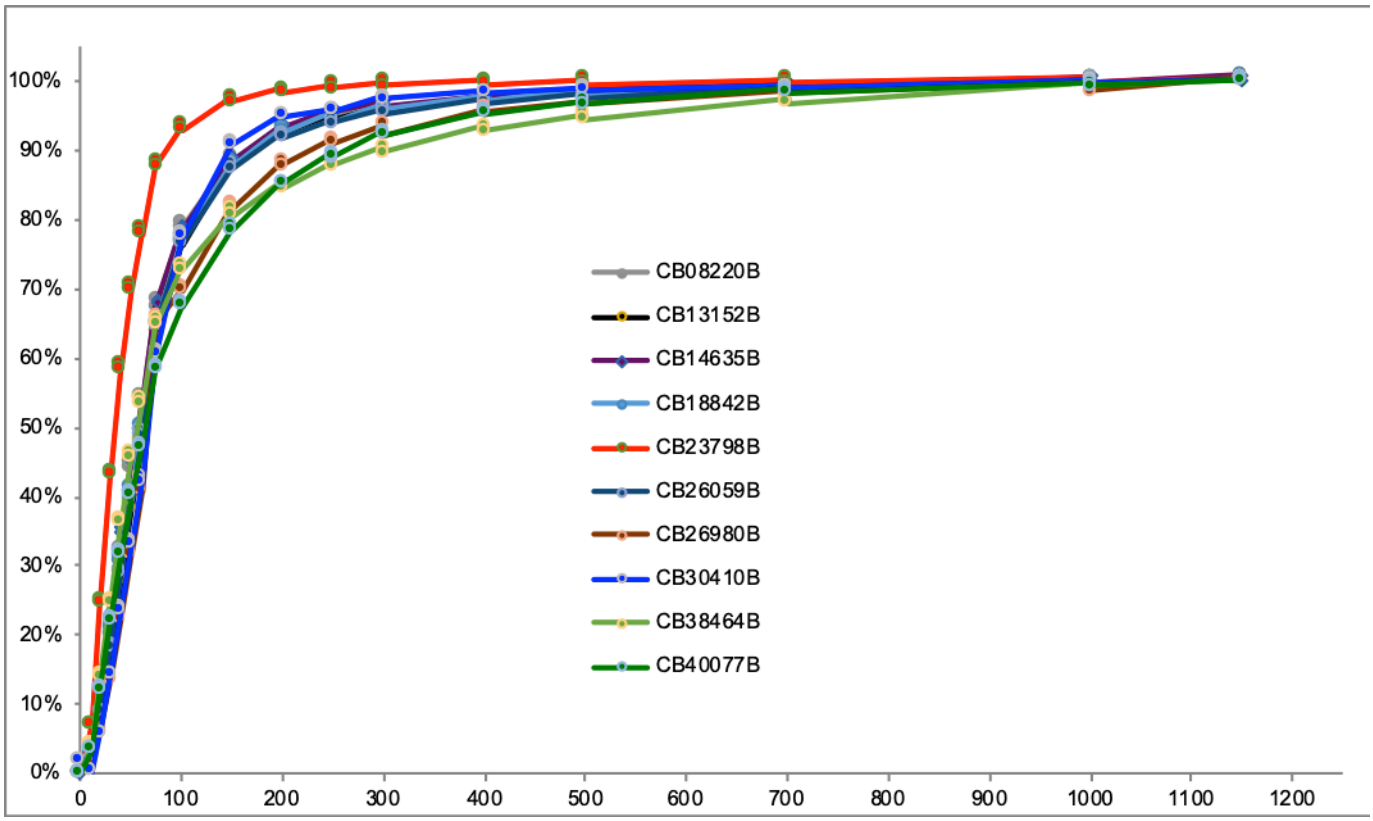

Figure S2a. Rock magnetic behaviours of 10 representative samples throughout the sampled interval. Isothermal Remanent Magnetization (IRM) acquisition at increasing fields in 50 mT steps up to 1200 mT.

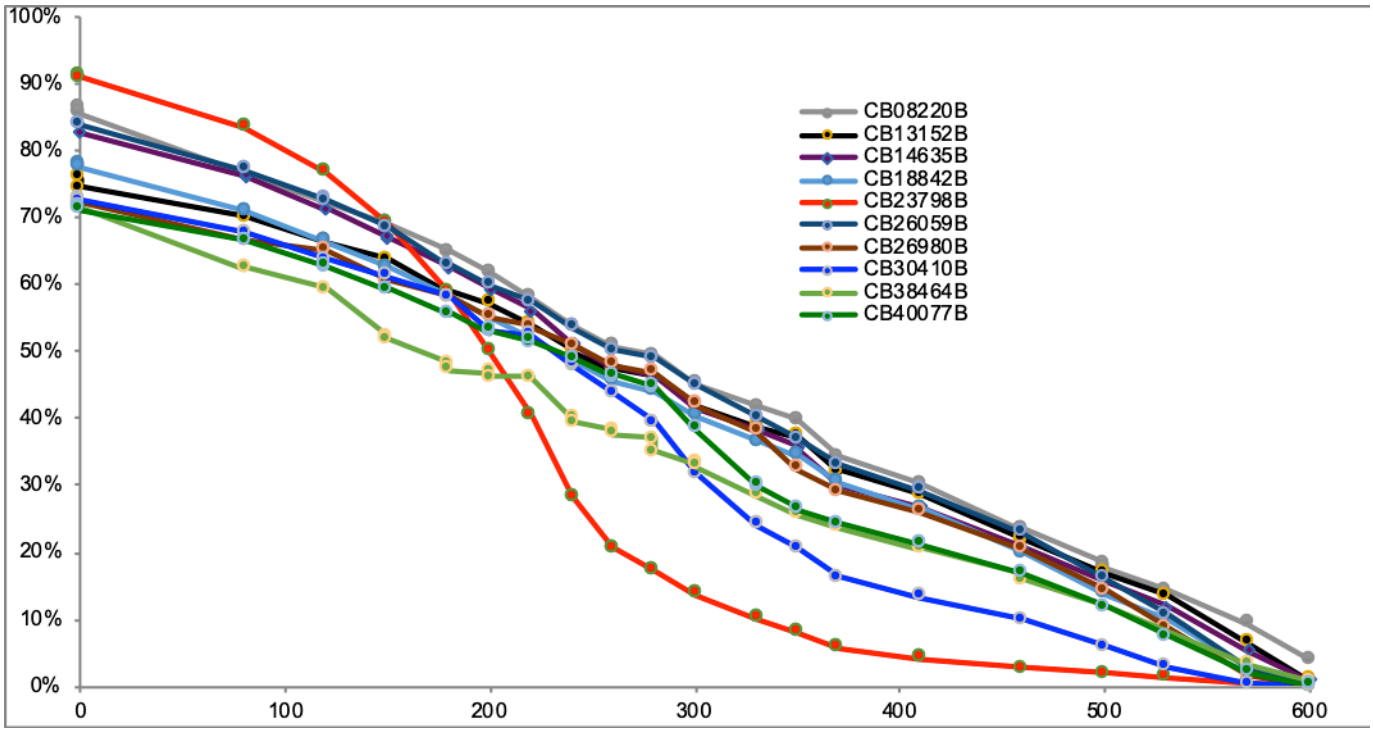

Figure S2b. Rock magnetic behaviours of 10 representative samples throughout the sampled interval. Thermal demagnetization at increasing temperatures up to 600°C of the soft coercivity component (<125 mT) expressed as it percentage of the total IRM.

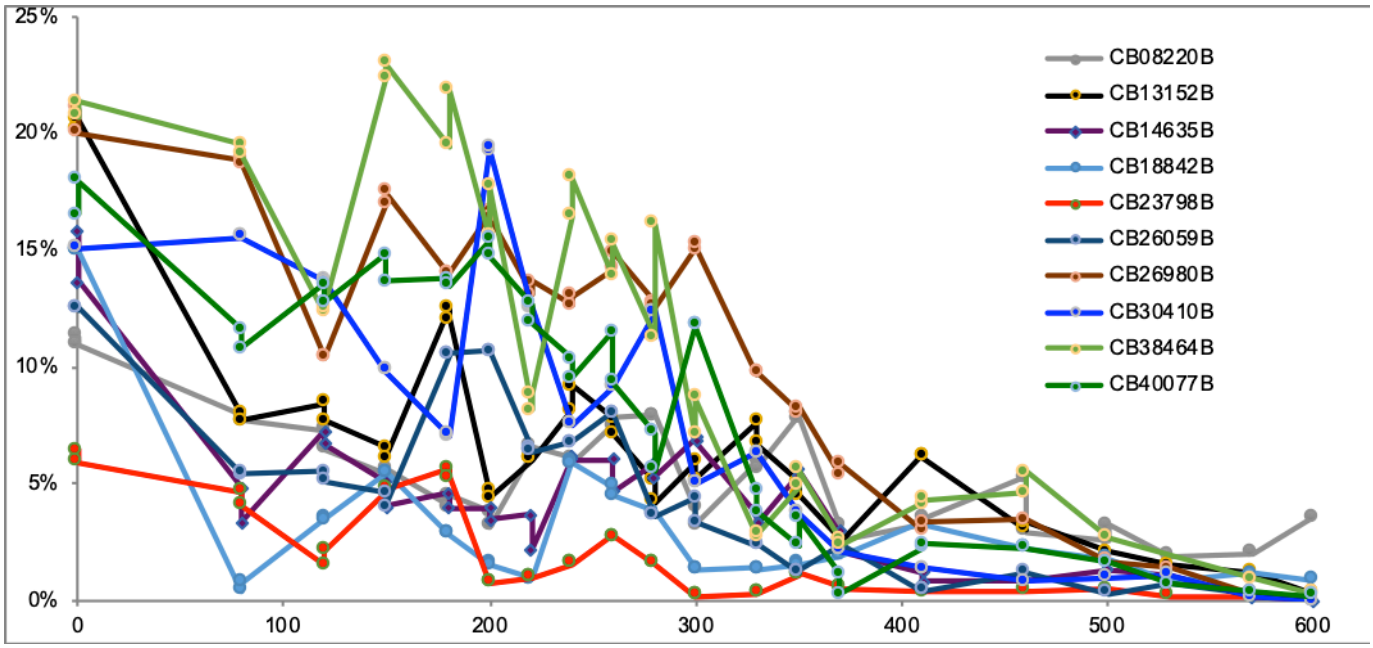

Figure S2c. Rock magnetic behaviours of 10 representative samples throughout the sampled interval. Thermal demagnetization at increasing temperatures up to 600°C of the intermediate coercivity component (125-400 mT) expressed as it percentage of the total IRM.

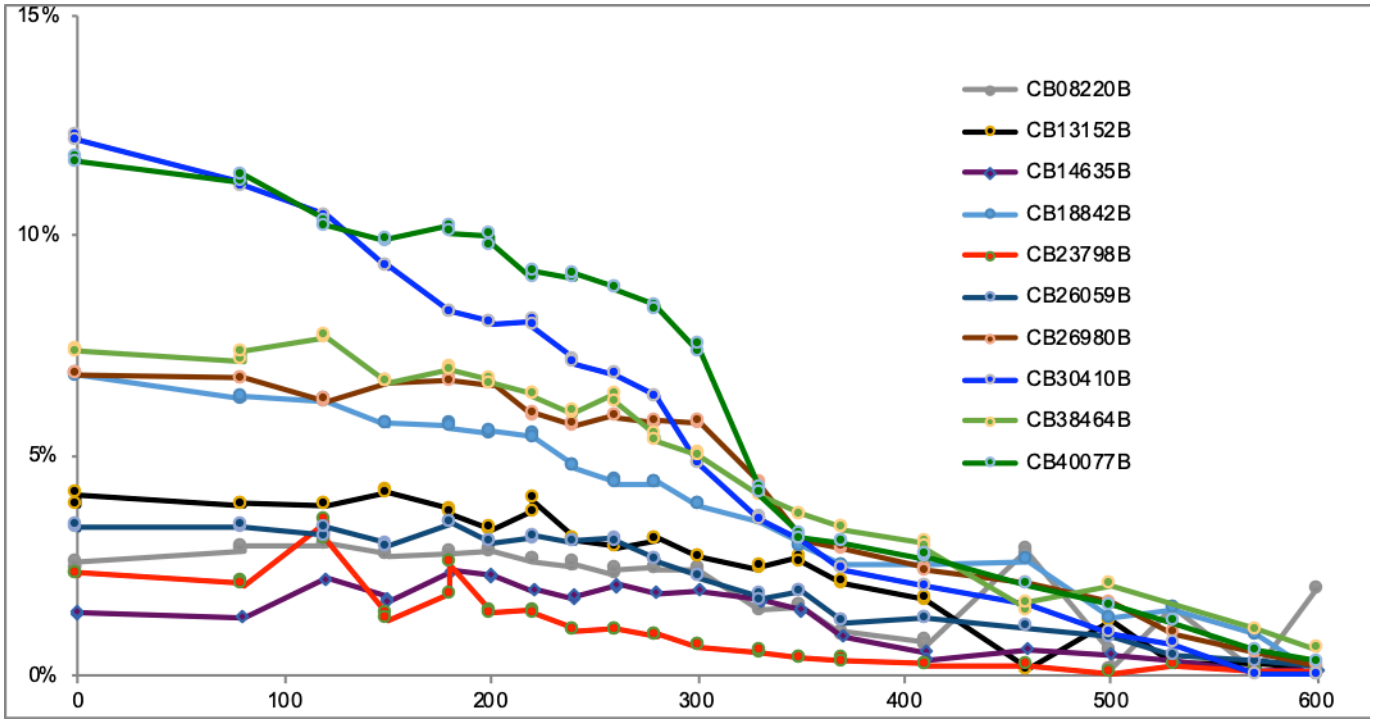

Figure S2d. Rock magnetic behaviours of 10 representative samples throughout the sampled interval. Thermal demagnetization at increasing temperatures up to 600°C of the strong coercivity component (400-1200 mT) expressed as it percentage of the total IRM.

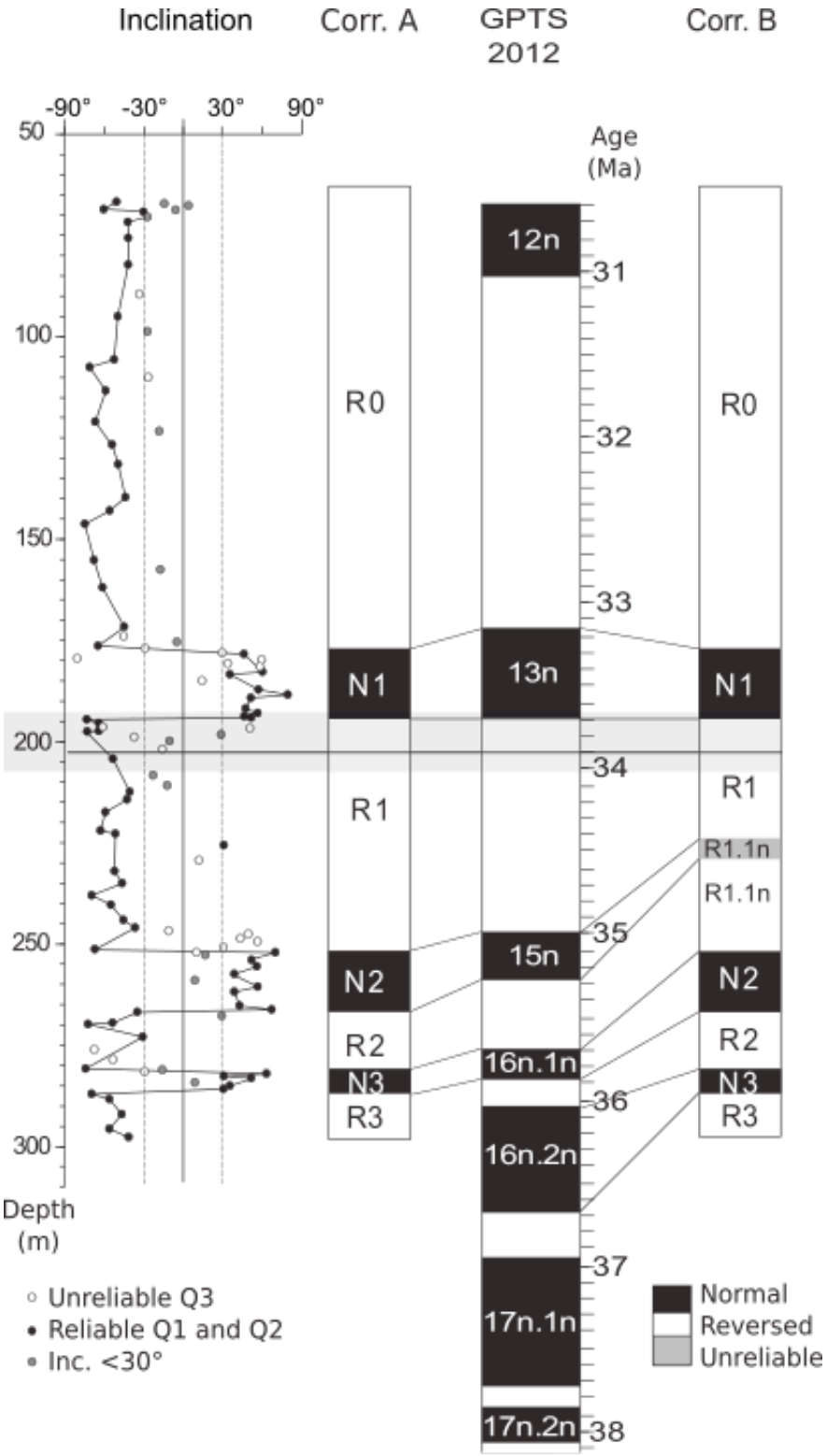

Figure S3. Magnetostratigraphic results and correlation to the Geomagnetic Polarity Time Scale (GPTS; Vandenberghe, 2012). Inclination - Inclinations of Characteristic Remanent Magnetizations from samples obtained though the stratigraphic depth. Positive (negative) inclinations indicate normal (reversed) polarities. Black symbols indicate reliable polarities (Qualities 1 and 2, see Fig. SI-1) and unreliable polarities are indicated in white (Quality 3, see Fig. SI-1) and grey for inclinations within ±30° that were systematically rejected. Polarity zones R0 to R3 and N1 to N3 are based on several consecutive reliable inclinations, R1.1n based on only one inclination is unreliable. EOB - Eocene-Oligocene Boundary indicated by grey area is defined by the

pollen transition in the stratigraphic log between 195.08 and 205.99m depth. Corr. A and Corr. B show proposed correlations to the GPTS. Correlation B including R1.1n is found unlikely. This polarity zone is defined by only 1 normal direction ca. 230 m depth. Correlating R1.1n with C15n would imply the above polarity zones N1 and R0 to correlate to C13n and C12r respectively, similar to correlation B. However, N2 and N3 below would have to correlate to C16n.1n and C16n.2n respectively although N2 is larger than N3 while C16n.1n is much shorter than C16n.2n. Also, R3 in between is much too large to account for the the short C16n.1r. Correlation B would imply unrealistic accumulation rate variations through the section such that it is clearly disfavored compared to the excellent fit provided by correlation A which is used for further analyses.

Depth (m)	Inc. (°)	MAD (°)	Q	Int. (10-5 A/m)	Susc. (10-5 SI)	Temp. (°C)	(m)	Reversal ±	(m)
66.70	-50.6	9.5	2	5.64	7	180-280			
67.18	-14.4	4.0	2	1.62	3	180-250			
67.54	4.0	3.9	2	3.35	8	180-300			
68.55	-60.5	9.3	2	2.11	2	180-320			
68.70	-5.7	12.2	2	3.80	3	200-340			
69.20	-30.2	10.2	2	0.93	3	180-320			
70.41	-27.2	4.0	2	2.56	5	200-300			
71.62	-42.0	7.4	2	0.76	7	180-260			
75.53	-41.7	2.8	2	31.20	9	180-260			
82.20	-41.8	5.5	2	2.21	10	240-330			
89.48	-33.1	8.9	3	1.92	12	200-240			
94.96	-49.7	5.0	2	6.16	13	180-280			
98.73	-27.3	14.1	1	3.40	10	330-450			
105.60	-52.5	5.3	2	2.57	3	240-370			
107.60	-71.2	15.9	1	2.06	9	240-370			
110.03	-26.5	21.5	3	4.89	15	220-250			
113.42	-58.8	12.7	2	0.92	17	200-330			
121.10	-66.7	11.7	2	1.46	16	200-300			
123.32	-18.3	15.5	2	2.08	17	200-330			
126.69	-54.1	7.5	2	2.32	9	200-330			
131.52	-49.5	13.2	2	2.04	11	200-260			
139.69	-44.0	14.5	1	4.25	7	220-370			
143.06	-55.9	4.0	1	19.76	11	180-350			
146.35	-74.9	19.9	1	19.53	9	240-330			
155.20	-67.7	4.6	2	2.02	13	200-240			
157.60	-17.5	30.4	2	3.14	14	180-250			
161.90	-61.3	9.2	2	0.94	15	200-350			
171.66	-44.9	11.7	2	1.21	16	200-350			
174.08	-45.0	13.8	3	2.93	18	180-280			
175.48	-4.8	4.1	1	4.69	14	180-300			
176.41	-64.7	12.2	2	1.22	13	240-340			
176.93	-28.9	13.8	3	3.26	17	200-320			
178.05	29.5	13.3	3	2.31	11	270-340			

178.46	46.1	8.8	2	4.43	12	180-300	**177.44**	**±**	**1.03**
179.48	-80.6	8.7	3	3.02	10	230-250			
179.82	59.5	14.6	3	3.89	13	0-200			
180.82	33.7	8.0	3	5.47	9	250-280			
181.49	58.4	4.5	3	5.03	7	230-250			
182.80	60.2	15.0	1	9.79	6	180-360			
183.39	35.4	3.5	1	20.06	6	180-330			
185.07	14.5	7.0	3	4.43	13	200-230			
187.20	57.0	4.1	2	4.53	7	180-250			
188.42	79.3	25.1	1	4.83	5	80-300			
189.22	51.4	3.8	1	19.62	9	180-350			
191.88	47.3	22.1	1	12.26	8	200-370			
192.94	56.3	5.2	1	10.70	9	180-350			
193.79	46.4	2.6	1	47.41	11	180-350			
194.15	51.6	3.9	1	10.75	12	180-360			
194.62	-73.2	4.0	1	98.09	11	180-350	**194.39**	**±**	**0.23**
195.58	-64.2	4.5	1	175.04	15	180-350			
196.51	-61.1	17.7	3	3.31	14	180-230			
196.80	50.6	22.2	3	1.93	13	250-340			
197.33	-64.0	2.0	1	204.79	13	180-350			
197.59	-72.8	11.6	2	1.33	12	240-350			
198.33	28.7	19.1	2	1.27	13	220-300			
198.95	-37.4	30.5	3	2.30	13	180-280			
199.88	-10.4	3.8	2	1.71	12	200-300			
202.01	-15.9	14.1	3	5.39	10	180-230			
204.23	-53.3	3.9	1	63.79	7	150-360			
208.30	-22.8	16.5	2	1.48	5	200-280			
210.85	-12.2	1.0	1	101.21	6	180-360			
212.44	-40.7	9.9	2	3.35	2	180-250			
214.35	-42.6	26.3	1	2.74	7	200-330			
217.39	-59.2	6.9	1	9.08	7	180-340			
222.06	-62.9	10.7	2	1.98	6	220-340			
222.73	-51.6	4.5	2	19.89	7	180-320			
225.55	30.8	6.1	1	3.57	1	180-360			
229.35	11.9	21.6	3	0.65	14	180-270			
231.98	-52.2	3.0	2	7.59	10	150-280			
235.03	-46.4	7.1	1	125.53	8	180-350			
237.98	-69.5	8.4	1	248.04	14	220-370			
240.33	-54.9	12.3	2	74.69	8	220-340			
244.08	-45.5	5.3	2	7.50	6	180-350			
245.99	-36.7	28.3	2	0.92	4	150-330			
246.82	-11.1	3.9	3	1.98	5	240-260			
247.61	49.3	6.2	3	11.47	2	180-280			

248.71	43.4	9.1	3	4.83	4	200-240			
249.48	56.3	12.9	3	8.67	8	180-280			
250.80	30.5	9.2	3	6.90	10	200-280			
251.34	-67.0	4.4	1	49.57	8	180-350			
252.04	69.7	1.4	1	156.05	7	180-360	**251.69**	**±**	**0.35**
252.16	10.1	5.1	3	8.91	6	250-350			
252.72	16.9	16.7	1	9.52	6	260-330			
254.05	51.9	8.8	1	12.87	6	180-330			
255.49	55.8	5.3	1	11.62	7	180-350			
257.37	38.6	4.0	1	8.88	9	180-350			
259.07	8.9	5.0	2	24.77	8	180-260			
260.59	56.4	14.2	1	15.84	5	150-370			
261.90	38.7	4.7	1	23.13	5	180-330			
265.29	42.6	4.5	1	13.84	7	180-350			
266.17	67.0	9.0	1	1.96	8	180-340			
266.91	-33.7	5.3	2	11.45	8	200-350	**266.54**	**±**	**0.37**
267.72	29.3	13.1	2	1.44	8	180-300			
269.58	-53.5	3.1	1	15.93	2	180-360			
269.80	-72.4	9.6	1	3.24	1	260-450			
273.02	-30.9	13.6	2	3.94	4	180-280			
276.02	-67.4	7.7	3	2.49	20	180-230			
278.59	-53.4	7.3	3	2.64	14	280-350			
280.79	-74.2	7.1	2	5.01	13	180-250			
281.14	-15.9	19.4	2	4.73	8	180-320			
281.59	-29.4	12.8	3	3.05	10	200-300			
282.10	63.1	8.3	1	6.52	10	220-320	**281.45**	**±**	**0.66**
282.66	31.0	7.0	2	8.44	10	180-250			
283.15	51.7	2.9	1	11.56	11	200-360			
284.17	9.0	6.6	2	27.30	15	220-340			
285.10	35.4	20.6	2	1.76	5	200-280			
285.85	30.5	6.5	2	3.27	3	220-280			
287.08	-69.4	3.1	1	1.70	21	180-350	**286.47**	**±**	**0.61**
288.36	-56.2	9.5	2	11.30	10	180-250			
292.12	-46.7	12.2	2	5.16	6	180-280			
295.63	-56.3	4.4	1	4.27	4	180-350			
297.76	-41.5	6.7	2	7.14	5	180-330			

Table S3. Depth - Stratigraphic depth below surface in meters; **Inc.** - Inclination of Characteristic Remanent direction determined from demagnetization path (ChRM); **MAD** - Maximum Angular Deviation from line fit of demagnetization path to determine ChRM direction; **Q** - Quality of ChRM inclination, 1 for Quality 1 with reliable direction and polarity, 2 for Quality 2 with reliable polarity but unreliable direction, 3 for Quality 3 with unreliable direction and polarity; **Int.** - Magnetic intensity of determined ChRM direction; **Susc.** - Magnetic Susceptibility of Natural Remanent Magnetization (NRM); **Temp.** -Temperature range used to determine ChRM direction; **Reversal** - Stratigraphic position of identified reversals positioned between 2 successive reliable directions of opposite polarities.

S3. Cyclostratigraphy

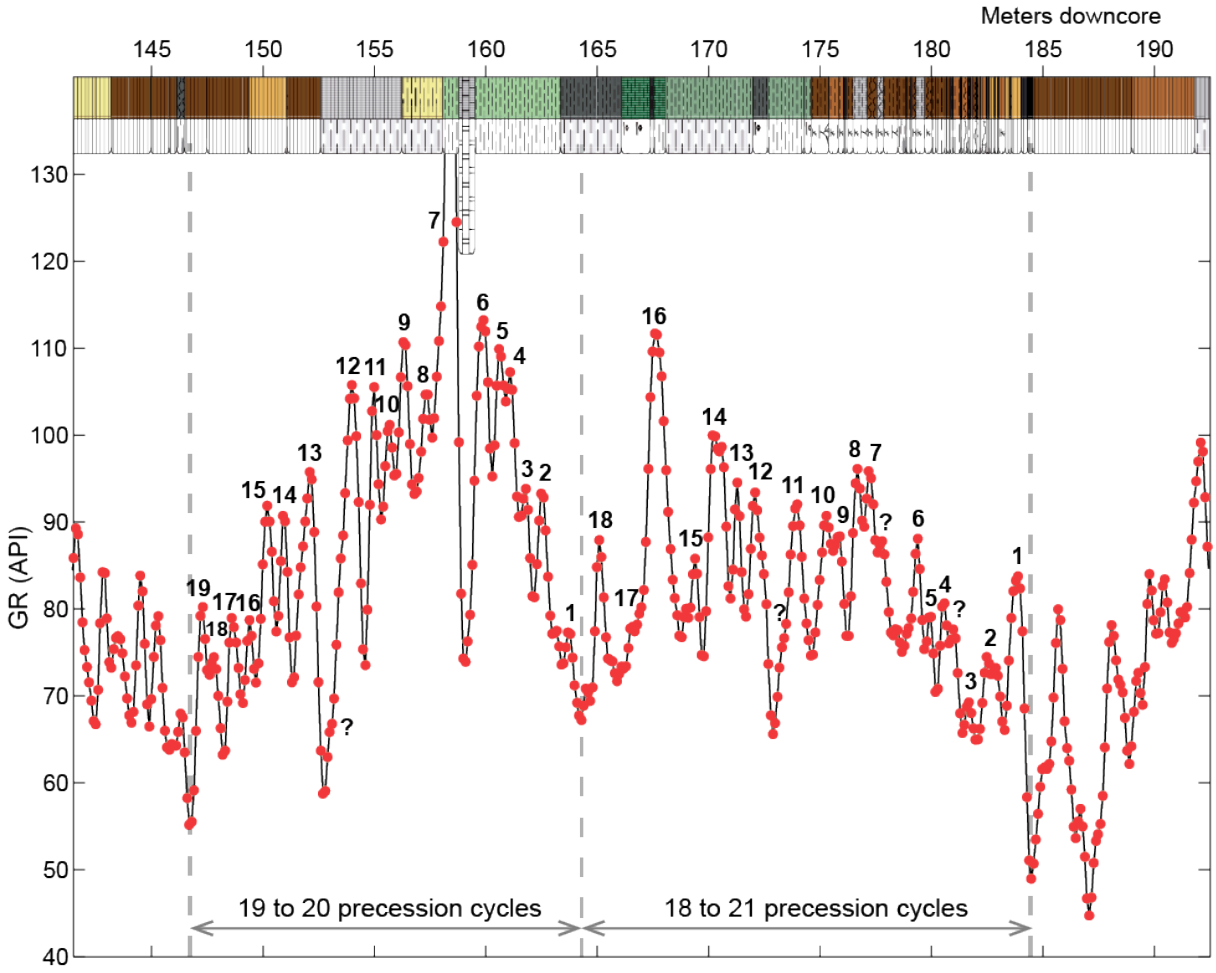

Figure S4. Illustration of counting of meter-scale cycles (precession) within the ~20 m cycles (405 kyr eccentricity) in interval I1. The vertical dashed lines delimit the ~20 m cycles.

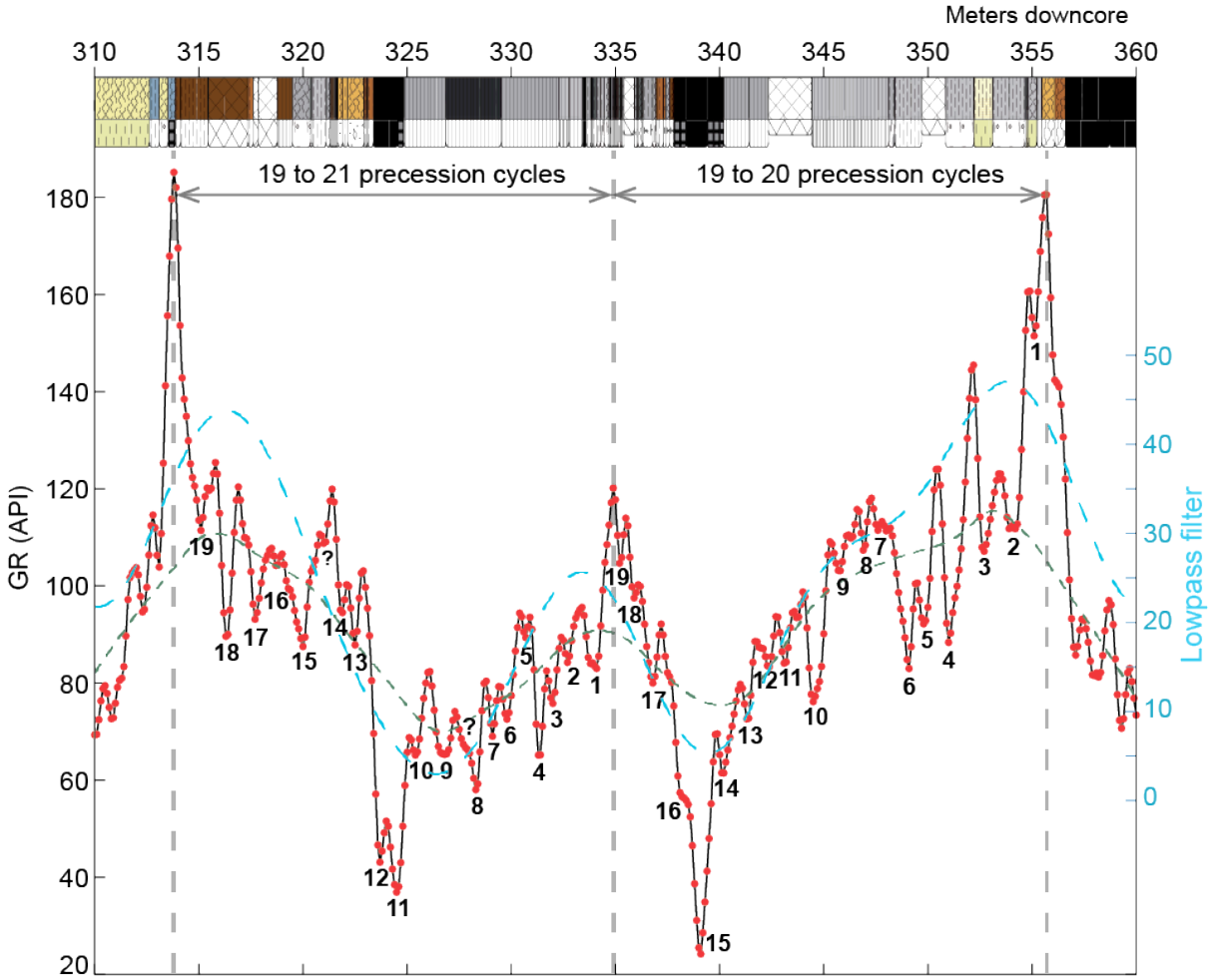

Figure S5. Illustration of counting of meter-scale cycles (precession) within the ~20 m cycles (405 kyr eccentricity) in interval I2. The vertical dashed lines delimit the ~20 m cycles. A low-pass filtering and a smoothing are applied to highlight the ~20 m cycles.

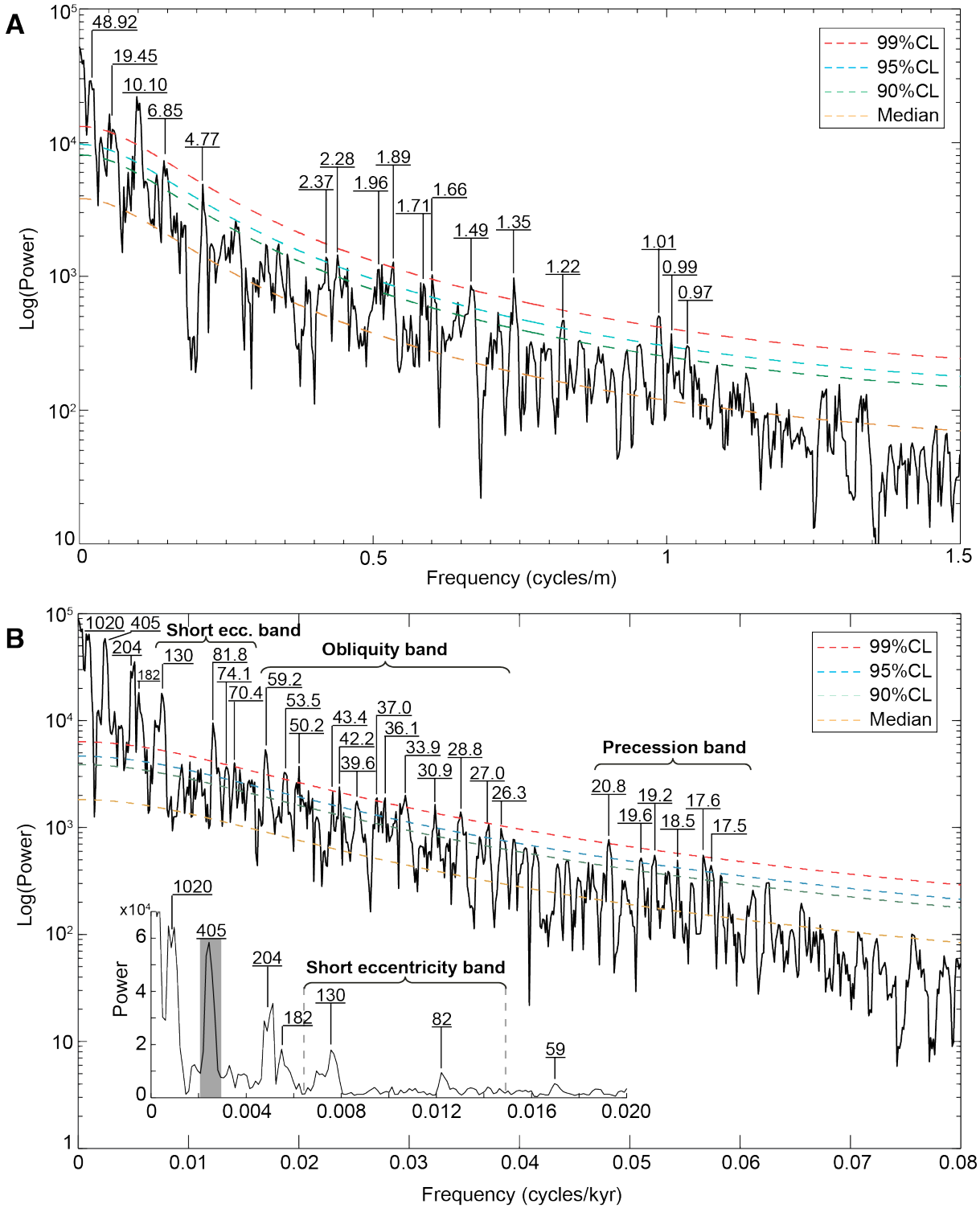

Figure S6. Time-series analysis of the untuned and tuned gamma-ray variations for the interval from 65.5 to 406 m. **(A)** 2π-MTM power spectrum of the untuned raw GR. Spectral periods are expressed in meters. **(B)** 2π-MTM power spectrum of the 405 kyr tuned GR. Spectral periods are expressed in kiloyears. *Inset*: spectrum over [0, 0.02 cycles/kyr] to show the low-frequency portion of the spectrum, with the grey-shaded peak corresponds to the target period for tuning.

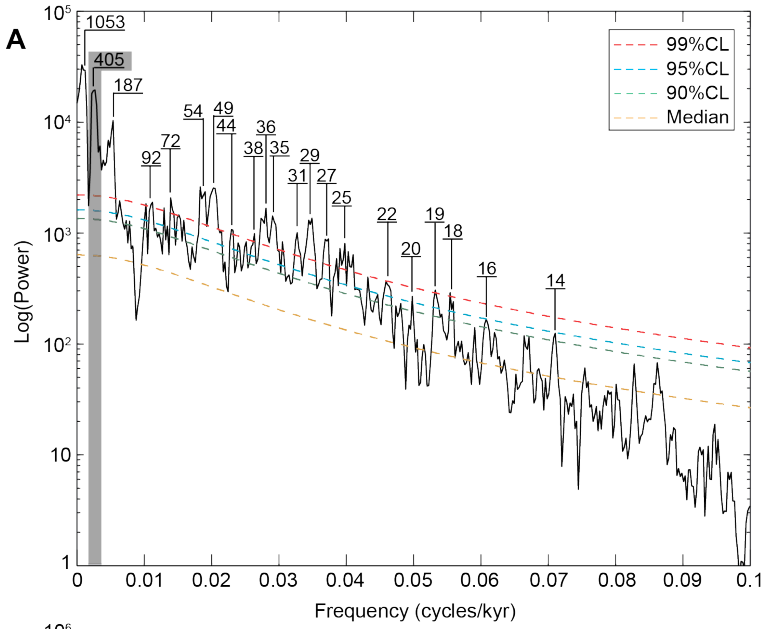
A
1053
405
187
92
72
54
49
44
38
36
35
31
29
27
25
22
20
19
18
16
14
99%CL
95%CL
90%CL
Median
Log(Power)
Frequency (cycles/kyr)

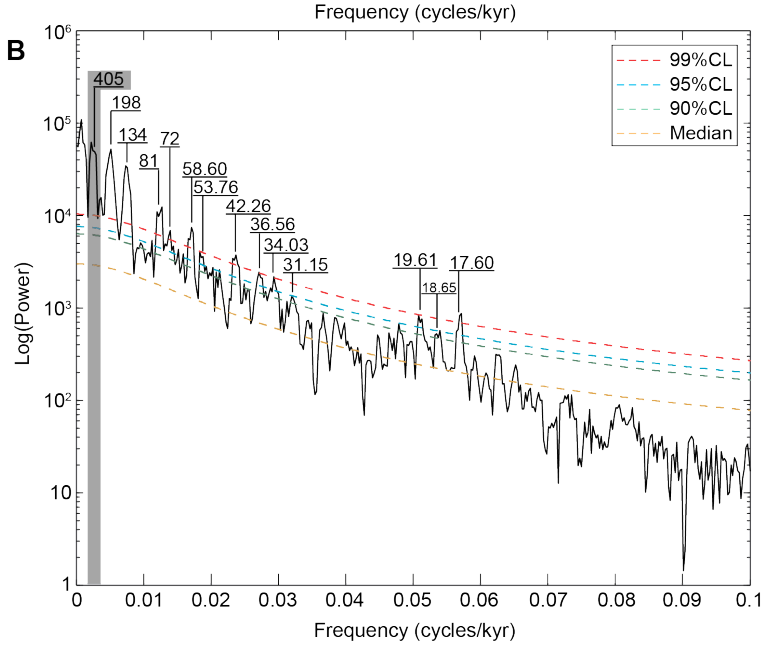
B
405
198
134
72
81
58.60
53.76
42.26
36.56
34.03
31.15
19.61
18.65
17.60
99%CL
95%CL
90%CL
Median
Log(Power)
Frequency (cycles/kyr)

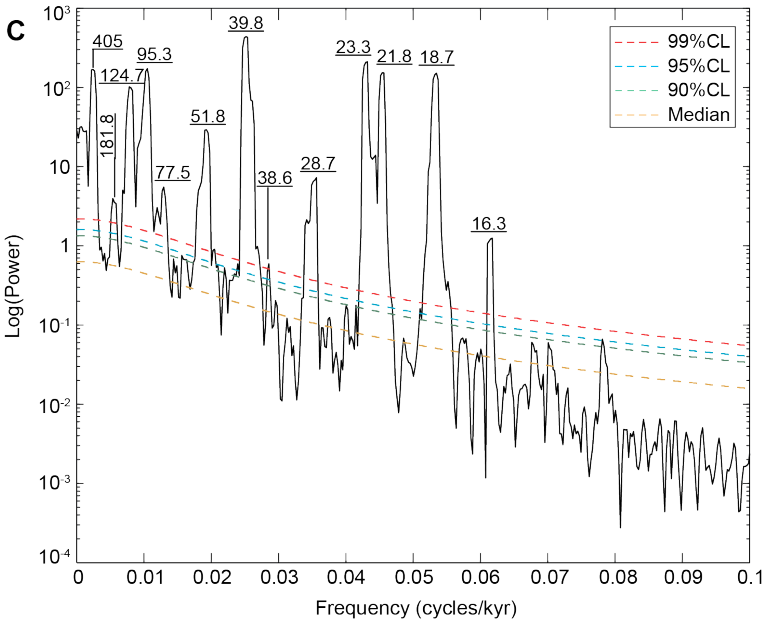
C
405
95.3
124.7
181.8
77.5
51.8
39.8
38.6
28.7
23.3
21.8
18.7
16.3
99%CL
95%CL
90%CL
Median
Log(Power)
Frequency (cycles/kyr)

Figure S7. Time-series analysis of the tuned gamma-ray (GR) variations per intervals I1 and I2 (as in Fig. 2 but in time domain) and comparison with astronomical frequencies. **(A)** 2π-MTM power spectrum of interval I1. **(B)** 2π-MTM power spectrum of interval I2. Grey-shaded vertical bars in 'A' and 'B' indicate the target 405 kyr periodicity used to time-calibrate the GR data. **(C)** 2π-MTM power spectrum of the La2004 astronomical variations (Laskar et al., 2004) in ETP format (Eccentricity, Tilt, Precession, e.g., Imbrie et al., 1984, pp. 296–297) for the interval from 31.065 to 34.710 Ma, roughly corresponding to the studied time interval I1. All spectral periods are expressed in kiloyears.

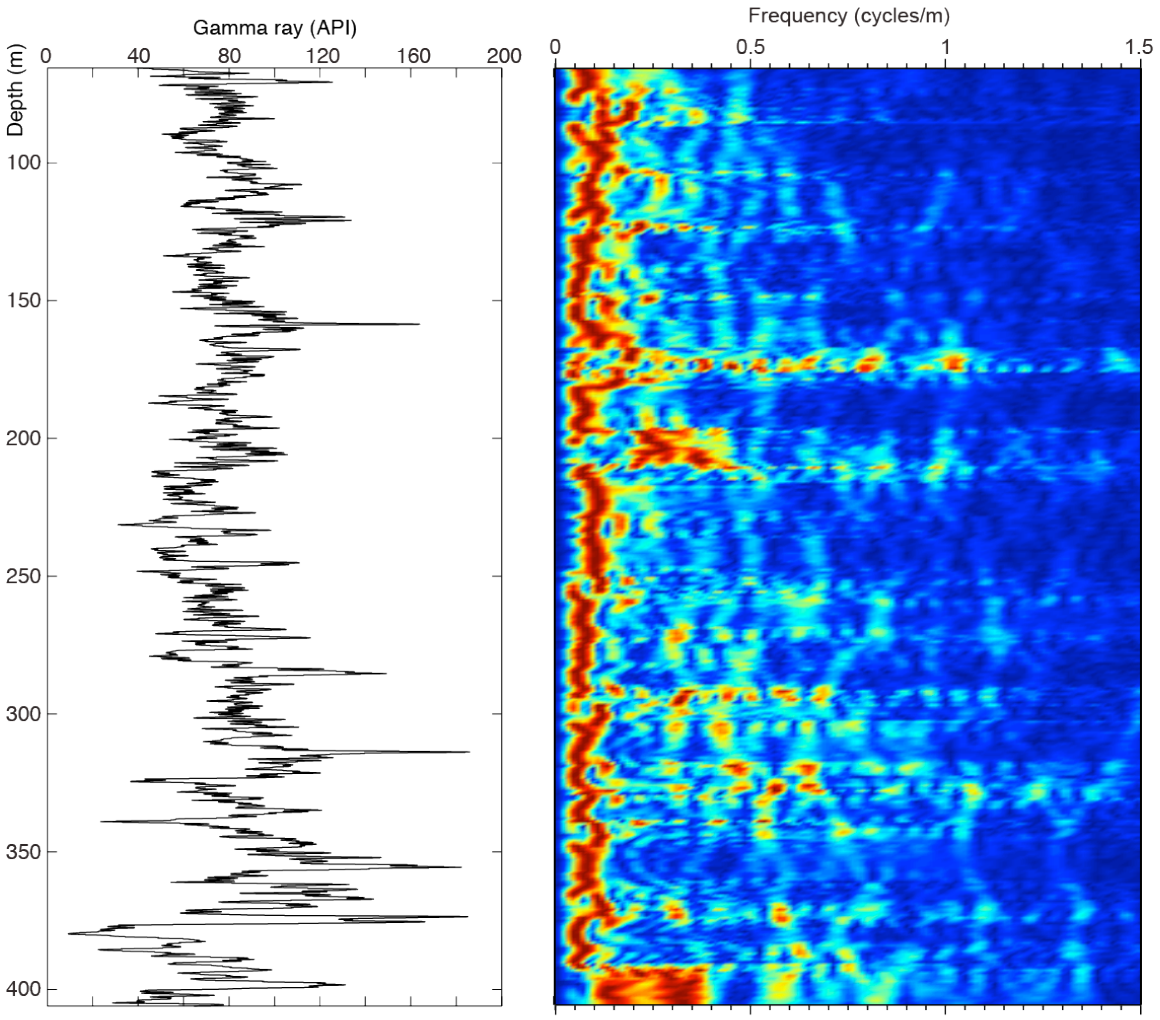

Figure S8. Evolutive harmonic analysis (EHA) of the untuned raw gamma-ray variations for the interval from 65.5 to 406 m. Spectral line indicates the ~20 m thick cycles. EHA options: window = 20 m, step = 0.1 m.

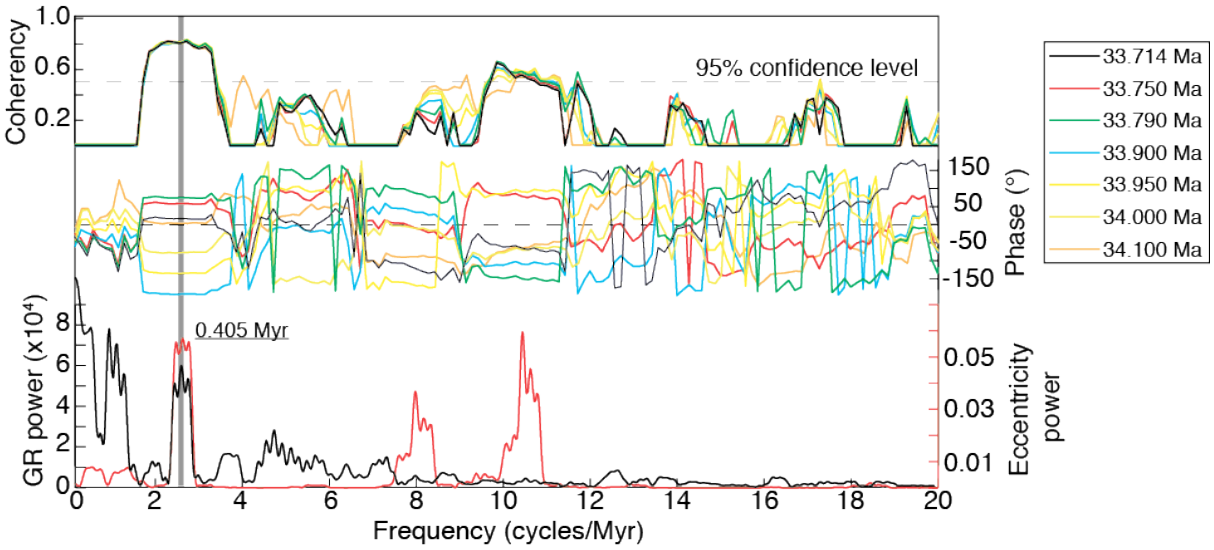

Figure S9. Coherency and cross-phase spectral analysis of the 405 kyr tuned gamma-ray data (GR) anchored at different ages of the Eocene–Oligocene boundary (tested ages and assoicated color coding in upper right panel, see Table S3 for references) versus the raw orbital eccentricity (Laskar et al., 2004). The approximate 95% confidence level for the coherency between red noise and a narrow band signal is indicated by the grey dashed line; the zero phase line is indicated by the black dashed line. Note the high coherency and phase relationship at the 405 kyr periodicity at the vertical grey shaded bar.

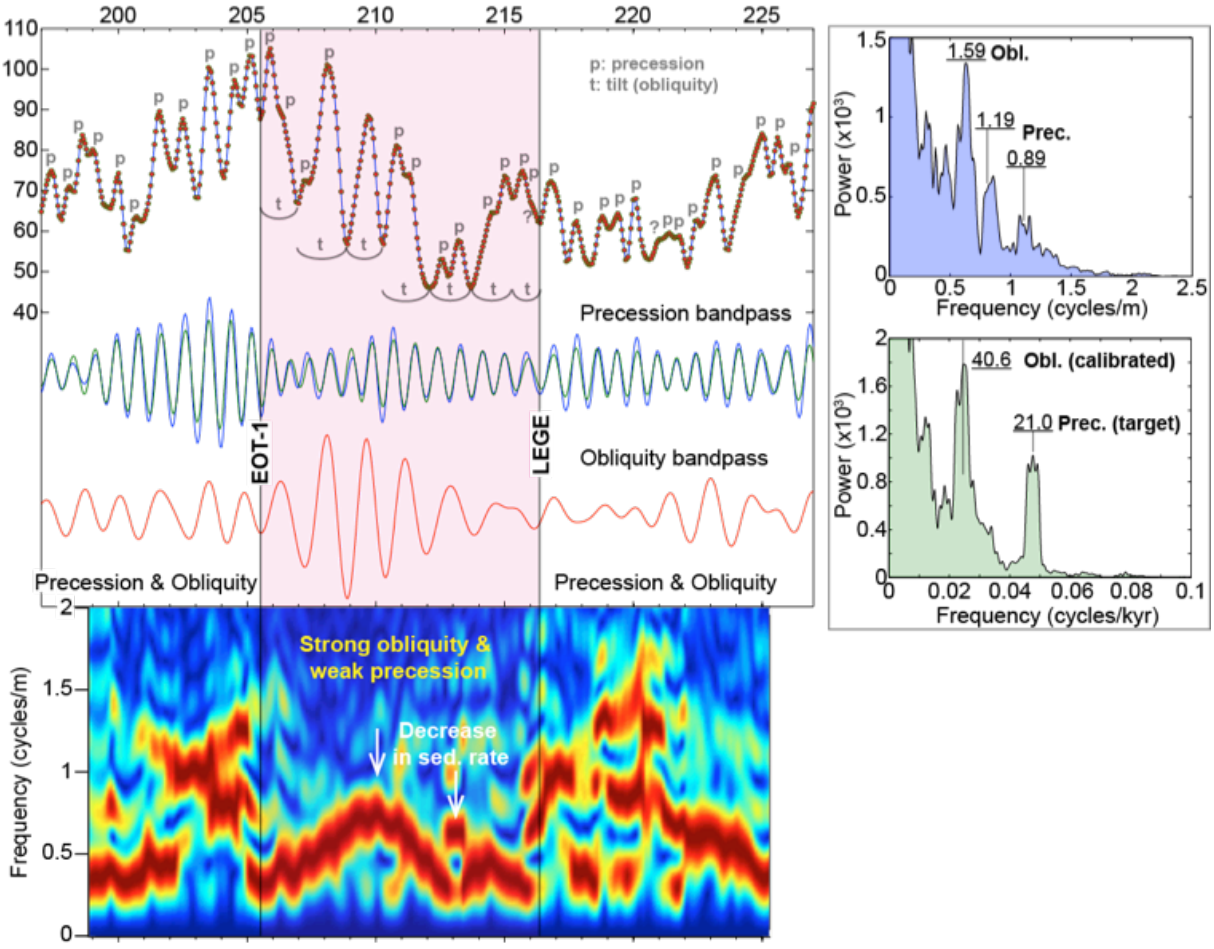

Figure S10. Evolutive harmonic analysis (EHA) of the untuned raw gamma-ray variations along with precession and obliquity bandpass filtering for the interval from 197 to 227 m to show the dominance of the obliquity, starting at around 216.5 m and ending at 195.5 m. These two core depths are interpreted as stratigraphically equivalent to the Late Eocene Glacial Event (LEGE) and the Eocene-Oligocence Transition event 1 (EOT-1). EHA options: window = 3.5 m, step = 0.1 m. Left panel: 2pi-MTM power spectra of the raw GR data (upper) and the 21 kyr tuned GR (lower). Note the successful calibration of the obliquity peak (of 1.59 m) to a period of 40.6 kyr.

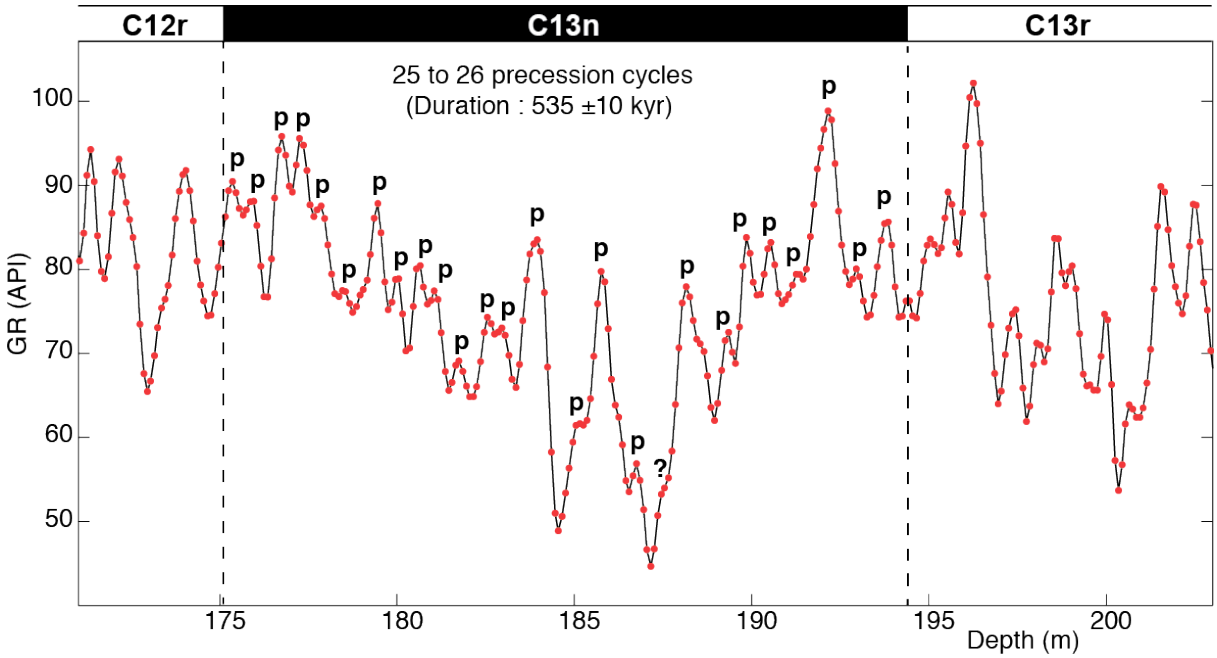

Figure S11. Example of precession cycle counting used as high-order tuning whenever the 405 kyr eccentricity cycle are seemingly complete (see 'strategy of tuning' in Section 4.3).

Authors/Section	Site 1218	Massignano	Massicore	Monte Cagnero	PEAT sites
Coxall et al. (2005)	33.90				
Pälike et al. (2006)	33.791				
Jovane et al. (2006)		33.714			
van Mourik et al. (2006)			33.75 (Option 1)		
van Mourik et al. (2006)			34.1 (Option 2)		
Brown et al. (2009)		33.90 ±0.01			
Hyland et al. (2009)				33.95	
Westerhold et al. (2014)					33.89

Table S4. Astronomical ages for the Eocene/Oligocene boundary used for cross-correlation.

S.4 References:

Bauer et al. (2016) The Cenozoic history of the Armorican Massif: New insights from the deep CDB1 borehole (Rennes Basin, France). C.R. Géoscience (accepted). doi 10.1016/j.crte.2016.02.002.

Berggren W. A., Kent, D. V., Swisher, C. C., III, and Aubry, M.-P., 1995, A revised Cenozoic geochronology and chronostratigraphy: In Berggren, W. A., Kent, D. V., Aubry, M.-P. and Hardenbol, J., (eds.), Geochronology Time Scales and Global Stratigraphic Correlation, Society of Economic Paleontologists and Mineralogists Special Publication N°. 54, pp. 129–212.

Brown, R.E., Koeberl, C., Montanari, A., Bice, D.M. 2009. Evidence fora change in Milankovitch forcing caused by extraterrestrial events at Massignano, Italy, Eocene-Oligocene boundary GSSP. Special Paper of the Geological Society of America*,* 452*, 119-137.*

Cahuzac, B., Poignant, A., 1997. Essai de biozonation de l'Oligo-Miocène dans les bassins européens à l'aide des grands foraminifères néritiques. Bull. Soc. Géol. Fr., 168, 155–169.

Cavelier, C., Le Calvez, Y. (1965) Présence d'Arenagula kerfornei (Allix), foraminifère 'biarritzien', a la partie terminale du Lutétien supérieur de Foulangues (Oise). Bulletin de la Société Géologique de France 7.2 (1965): 284-286.

Châteauneuf, J.J., 1980. Palynostratigraphie et paléoclimatologie de l'Eocène supérieur et de l'Oligocène du Bassin de Paris (France). Mém. BRGM, 116, 357 p.

Coxall, H.K., Wilson, P.A., Pälike, H., Lear, C.H., Backman, J., 2005. Rapid stepwise onset of Antarctic glaciation and deeper calcite compensation in the Pacific Ocean. Nature 433, 53–57.

Ghirardi, J., 2016. Impact de la transition climatique Eocène-Oligocène sur les écosystèmes continentaux, Etude du Bassin de Rennes. PhD thesis, Université d'Orléans, France.

Herron, S.L., 1991. In situ evaluation of potential source rocks by wireline logs, In: Merrill, R.K. (Ed.), Source and Migration Processes and Evaluation Techniques: AAPG Treatise of Petroleum Geology. Handbook of Petroleum Geology 1, 127–134.

Hesselbo, S.P., 1996. Spectral gamma-ray logs in relation to clay mineralogy and sequence stratigraphy, Cenozoic of the atlantic margin, offshore new jersey. In: Mountain, G.S., Miller, K.G., Blum, P., Poag, C.W., Twichell, D.C. (Eds.), Proceedings of the Ocean Drilling Program, Scientific Results 150, 411-422.

Hottinger L., Schaub, H. (1960): Zur Stufeneinteilung des Paleocaens und des Eocaens. Einführung der Stufen Ilerdien und Biarritzien. Eclogae geol. Helv. 53/1, 453-479.

Hyland, E., Murphy, B., Varela, P., Marks, K., Colwell, L., Tori, F., Monechi, S., Cleaveland, L., Brinkhuis, H., van Mourik, C.A., Coccioni, C., Bice, D., Montanari, A., 2009. Integrated stratigraphy and astrochronologic calibration of the Eocene-Oligocene transition in the Monte Cagnero section (northeastern Apennines, Italy): A potential parastratotype for the Massignano GSSP, in Koeberl, C., Montanari, A. (Eds.), The Late Eocene Earth—Hothouse, Icehouse, and Impacts. Geol. Soc. Am. Sp. Pap. 452, 303–322.

Imbrie, J., Hays, J.D., Martinson, D.G., McIntyre, A., Mix, A.C., Morley, J.J., Pisias, N.G., Prell, W.L., Shackleton, N.J., 1984. The orbital theory of Pleistocene climate: support from a revised chronology of the marine ä^{18}O record, in: Berger A. *et al.* (Eds.), Milankovitch and climate, Understanding the response to astronomical forcing NATO. Adv. Sc. Inst. Ser. C. 126, 269-305.

Ionescu A., Alexandrescu, G. (1995) *Boehlensipollis hohli* in the lower Oligocene bituminous formation from Trotusului Valley (East Carpathians). Romanian Journal of Palaeontology, 76:67-72

Jovane, L., Florindo, F., Sprovieri, M., Pälike, H., 2006. Astronomic calibration of the late Eocene/early Oligocene Massignano section (central Italy). Geoch. Geophys. Geosys. 7, doi: 10.1029/2005GC001195.

King, 2016. A Revised Correlation of Tertiary Rocks in the British Isles and Adjacent Areas of New Europe. Edited by A.S. Gale & T.L. Barry. Geological Society of London Special Report 27, 724 pp.

Köthe, A., 2003. Dinozysten-Zonierung im Tertiar Norddeutschlands. Revue de Paléobiologie 22, 895–923.

Köthe, A., 2005. Korrelation der Dinozysten-Zonen mit anderen biostratigraphisch wichtigen Mikrofossilgruppen im Tertiar Norddeutschlands. Revue de Paléobiologie 24, 697–718.

Köthe, A, 2012. A revised Cenozoic dinoflagellate cyst and calcareous nannoplankton zonation for the German sector of the southeastern North Sea Basin. Newsletters on Stratigraphy, 45, 189-220.

Köthe, A., Piesker, B., 2007. Stratigraphic distribution of Paleogene and Miocene dinocysts in Germany. Revue de Paleobiologie 26, 1–39.

Laskar, J., Robutel, P., Joutel, F., Gastineau, M., Correia, A.C.M., Levrard, B., 2004. A long-term numerical solution for the insolution quantities of the Earth. Astron. Astrophys. 428, 261–285.

Margerel, J.-P., 2009. Les foraminifères benthiques des Faluns du Miocène moyen du Blésois (Loir-et-Cher) et de Mirebeau (Vienne) dans le Centre-Ouest de la France. Geodiversitas 31 (3), 577–621.

Margerel J.-P., Bréhéret, J.-G., 1984. Révision de l'attribution stratigraphique du gi-sement de Chasné-sur-Illet (Ille-et-Vilaine) à l'aide de la faune de foraminifères et de la nannoflore calcaire. Cahiers de Micropaléontologie 1, 5–25.

McFadden, P.L., Reid, A., 1982. Analysis of paleomagnetic inclination data. Geophys. J. R. Astr. Soc. 69, 307-319.

Schuler, M. and C. Sittler. 1976. Présence d'un grain de pollen *Boehlensipollis hohli* W. Kr. 1962 dans les séries Tertiaires de la plaine du Forez (Massif Central). Attributions stratigraphiques nouvelles de ces terrains. Sci. Geol. Bull. 29: 91-92.

Palike, H., Norris, R.D., Herrle, J.O., Wilson, P.A., Coxall, H.K., Lear, C.H., Shackleton, N.J., Tripati, A.K., Wade, B.S., 2006. The Heartbeat of the Oligocene Climate System. Science 314, 1894–1898.

Serra-Kiel, J., Hottinger, L., Caus, E., Drabne, K., Ferrandez, C., Jauhri, A. K., Less, G., Pavlovec, R., Pignatti, J., Samso, J.-M., Schaub, H., Sirel, E., Strougo, A., Tambareau, Y., Tosquella, J., Zakrevskaya, E., 1998. Larger foraminiferal biostratigraphy of the Tethyan Paleocene and Eocene. Bull. Soc. Géol. Fr., 169, 281–299.

Sittler, C, Schuler, M., 1976. Extension stratigraphique, répartition géographique et écologie de deux genres polliniques paléogènes observés en Europe occidentale: Aglaoreidia et Boehlensipollis. Bull. Soc. Bot. Fr, 122, 231–254.

Sittler, C., Monique Schuler, C. Caratini, J. J. Chateauneuf, C. Gruas-Cavagnetto, S. Jardine, M. F. Ollivier, E. Roche & C. Tissot (1975) Extension stratigraphique, répartition géographique et écologie de deux genres polliniques paléogènes observés en Europe occidentale: *Aglaoreidia* et *Boehlensipollis*, Bulletin de la Société Botanique de France, 122:sup1, 231-245, DOI:10.1080/00378941.1975.10835657.

Van Vliet-Lanoë, B., Laurent, M., Hallégouët, B., Margerel, J.-P., Chauvel, J.- J., Michel, Y., Moguedet, G., Trautmann, F., Vauthier, S., 1998. Le Mio- Pliocène du Massif armoricain. Données nouvelles. C. R. Acad. Sci. Paris, Ser. IIa 326, 333–340.

Vandenberghe, N., Hilgen, F.J., Speijer, R.P., with contributions by Ogg, J.G., Gradstein, F.M., Hammer, O., Hollis, C.J., Hooker, J.J., 2012. The Paleogene Period. In: Gradstein, F.M., Ogg, J.G., Schmitz, M.D., Ogg, G.M. (Eds.), The Geological Time Scale 2012, vol. 2, Elsevier, pp. 855–921.

Van Mourik, C.A., Lourens, L.J., Brinkhuis, H., Pälike, H., Hilgen, F.J., Montanari, A., Coccioni, R., 2006. From greenhouse to icehouse at the Massignano Eocene-Oligocene GSSP: Implications for the cause, timing and effect of the Oi-1 glaciation, in: van Mourik, C.A. (Ed.), The Greenhouse-Icehouse Transition, A Dinoflagellate Perspective. Ph.D. thesis, Stockholm University, 327.

Westerhold, T., Röhl, U., Pälike, H., Wilkens, R., Wilson, P.A., Acton, G., 2014. Orbitally tuned timescale and astronomical forcing in the middle Eocene to early Oligocene. Clim. Past 10, 955-973.